Observation of Quantum Criticality with Ultracold Atoms in Optical Lattices

Xibo Zhang,* Chen-Lung Hung, Shih-Kuang Tung, Cheng Chin*

Quantum criticality emerges when a many-body system is in the proximity of a continuous phase transition that is driven by quantum fluctuations. In the quantum critical regime, exotic, yet universal properties are anticipated; ultracold atoms provide a clean system to test these predictions. We report the observation of quantum criticality with two-dimensional Bose gases in optical lattices. On the basis of in situ density measurements, we observe scaling behavior of the equation of state at low temperatures, locate the quantum critical point, and constrain the critical exponents. We observe a finite critical entropy per particle that carries a weak dependence on the atomic interaction strength. Our experiment provides a prototypical method to study quantum criticality with ultracold atoms.

In the vicinity of a continuous quantum phase transition, a many-body system enters the quantum critical regime, where quantum fluctuations lead to nonclassical universal behavior (*1*, *2*). Quantum criticality not only provides novel routes to new material design and discovery (*1*, *3*–*6*), but also provides a common framework for problems in condensed matter, nuclear physics (*7*, *8*), and cosmology (*1*, *9*). Quantum criticality plays a central role in strongly correlated systems such as heavy-fermion materials (*5*), spin dimer systems (*10*), Ising ferromagnets (*11*), and chromium at high pressure (*12*).

Ultracold atoms offer a clean setting for quantitative and precise investigation of quantum phase transitions (*13*–*16*) and critical phenomena (*17*). For example, the superfluid-to-Mott insulator quantum phase transition can be realized by loading atomic Bose-Einstein condensates into optical lattices (*13*). In recent experiments, scaling behavior of physical observables was reported in interacting Bose gases in three (*17*) and two dimensions (*18*), and in Rydberg gases (*19*), where collective behavior is insensitive to microscopic details. In addition, suppression of the superfluid critical temperature near the Mott transition was observed in three-dimensional (3D) optical lattices (*20*). Studying quantum criticality in cold atoms on the basis of finite-temperature thermodynamic measurements, however, remains challenging and has attracted increasing theoretical interest in recent years (*21*–*24*).

We report the observation of quantum critical behavior of ultracold cesium atoms in a two-dimensional (2D) optical lattice across the vacuum-to-superfluid transition. This phase transition can be viewed as a transition between a Mott insulator with zero occupation number and a superfluid, and can be described by the Bose-Hubbard model (*25*). Our measurements are performed on atomic samples near the normal-to-superfluid transition, connecting to the vacuum-to-superfluid quantum phase transition in the zero-temperature limit.

The quantum phase transition and quantum critical regime in this study are illustrated in Fig. 1. The zero-temperature vacuum-to-superfluid transition occurs when the chemical potential μ approaches its critical value μ_0. Sufficiently close to the quantum critical point, the critical temperature T_c for the normal-to-superfluid transition is expected to decrease according to the following scaling (*25*)

$$\frac{k_B T_c}{t} = c\left(\frac{\mu - \mu_0}{t}\right)^{z\nu} \quad (1)$$

where k_B is the Boltzmann constant, t is the tunneling energy, z is the dynamical critical exponent, ν is the correlation length exponent, and c is a constant. In the quantum critical regime (shaded area in Fig. 1), the temperature T provides the sole energy scale, and all thermodynamic observables are expected to scale with T (*25*). Thus, the equation of state is predicted to obey the following scaling (*21*)

$$\tilde{N} = F(\tilde{\mu}) \quad (2)$$

in which $F(x)$ is a generic function, and

$$\tilde{N} = \frac{N - N_r}{\left(\frac{k_B T}{t}\right)^{\frac{D}{z}+1-\frac{1}{z\nu}}} \text{ and } \tilde{\mu} = \frac{\frac{\mu-\mu_0}{t}}{\left(\frac{k_B T}{t}\right)^{\frac{1}{z\nu}}} \quad (3)$$

are the scaled occupation number and scaled chemical potential, respectively. Here, N is the occupation number, D is the dimensionality, and N_r is the nonuniversal part of the occupation number. For the vacuum-to-superfluid transition in the 2D Bose-Hubbard model, we have $N_r = 0$ and $D = 2$, and the predicted critical exponents are $z = 2$ and $\nu = 1/2$, characteristics of the dilute Bose gas universality class (*2*, *22*, *25*). We note that in a 2D system, there can be logarithmic corrections to scaling functions, including those in this study, near the quantum critical point (*2*). Within the temperature range of our experiment, however, the measurement is consistent with the above scaling laws in the absence of logarithmic corrections. Scaling behavior of T_c in the quantum critical regime was also observed in 2D condensates of spin triplets (*10*).

Our experiment is based on 2D atomic gases of cesium-133 in 2D square optical lattices (*26*, *27*). The 2D trap geometry is provided by the weak horizontal (r-) confinement and strong vertical (z-) confinement (*27*), with envelope trap frequencies f_r = 9.6 Hz and f_z = 1940 Hz, respectively. Typically, 4000 to 20,000 atoms are loaded into the lattice. The lattice constant is $d = \lambda/2 = 0.532$ μm and the depth is $V_L = 6.8\ E_R$, where $E_R = k_B \times 63.6$ nK is the recoil energy, $\lambda = 1064$ nm is the lattice laser wavelength, and h is the Planck constant. In the lattice, the tunneling energy is $t = k_B \times 2.7$ nK, the on-site interaction is $U = k_B \times 17$ nK, and the scattering length is $a = 15.9$ nm. The sample temperature is controlled in the range of 5.8 to 31 nK.

We determine the equation of state $n(\mu,T)$ of the sample from the measured in situ density distribution $n(x,y)$ (*18*, *26*). The chemical potential $\mu(x,y)$ and the temperature T are obtained by fitting the low-density tail of the sample where the atoms are normal. The fit is based on a mean-field model that accounts for interaction (*28*–*30*).

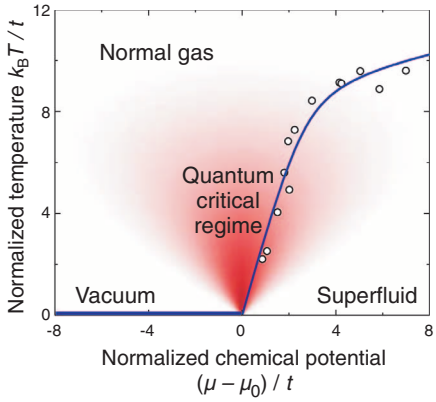

Fig. 1. The vacuum-to-superfluid quantum phase transition in 2D optical lattices. At zero temperature, a quantum phase transition from vacuum (horizontal thick blue line) to superfluid occurs when the chemical potential μ reaches the critical value μ_0. Sufficiently close to the transition point μ_0, quantum criticality prevails (red shaded area), and the normal-to-superfluid transition temperature T_c [measurements (*30*) shown as empty circles] is expected to vanish as $T_c \sim (\mu - \mu_0)^{z\nu}$; the blue line is a guide to the eye. From the prediction $z\nu = 1$ (*22*, *23*, *25*), the linearly extrapolated critical chemical potential is $\mu_0 = -3.6(6)t$, consistent with the theoretical value $-4t$ (*28*). Both the thermal energy scale $k_B T$ and the chemical potential μ are normalized by the tunneling t.

The James Franck Institute and Department of Physics, The University of Chicago, Chicago, IL 60637, USA.

*To whom correspondence should be addressed. E-mail: xibo@uchicago.edu (X.Z.); cchin@uchicago.edu (C.C.)

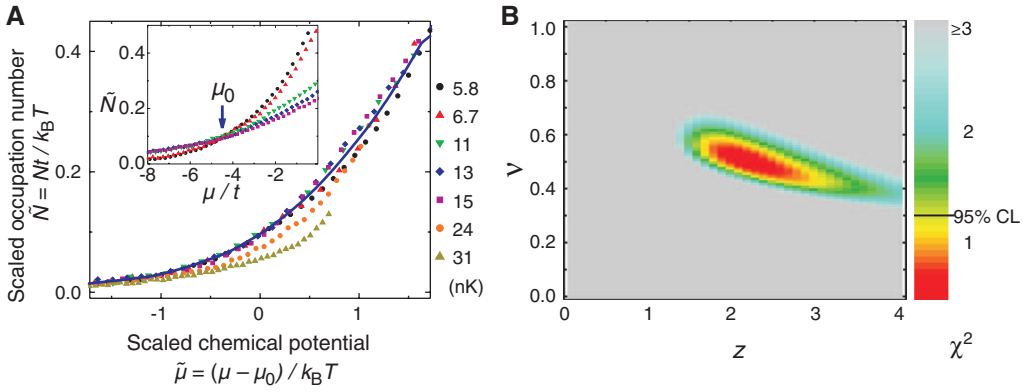

Fig. 2. Evidence of a quantum critical regime. (**A**) Scaled occupation number $\tilde{N} = Nt/k_BT$ as a function of the scaled chemical potential $\tilde{\mu} = (\mu - \mu_0)/k_BT$; the blue solid line shows the average curve for the lowest four temperatures. Inset shows the low-temperature data in the range of T = 5.8 to 15 nK, and the critical chemical potential μ_0 is identified as the crossing point; see text. The result, $\mu_0 = -4.5(6)\,t$, agrees with the prediction $\mu_0 = -4t$ (*28*). (**B**) Determination of the dynamical critical exponent z and the correlation length exponent ν based on $\mu_0 = -4.5t$. The color represents the reduced chi-squared (χ^2), and indicates how well the scaled equation of state can collapse into one single curve. The exponents are determined as $z = 2.2^{+1.0}_{-0.5}$ and $\nu = 0.52^{+0.09}_{-0.10}$, and the uncertainties correspond to a 95% confidence level. The predicted values are z = 2 and ν = 1/2.

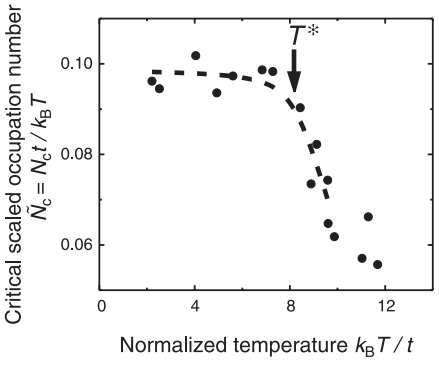

Fig. 3. Finite-temperature effect on quantum critical scaling. Scaled occupation number $\tilde{N}_c = N_c t/k_BT$ at the critical chemical potential $\mu = \mu_0$ as a function of the normalized temperature k_BT/t. The black dashed line is an empirical fit, giving a temperature scale $T^* \approx 8t/k_B$. For $T < T^*$, $\tilde{N}_c \approx 0.097$ is independent of the temperature; for $T > T^*$, $\tilde{N}_c$ deviates from the low-temperature value.

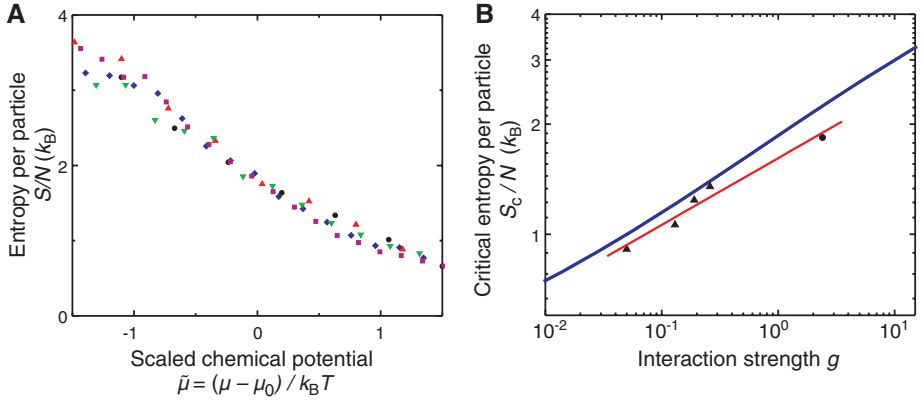

Fig. 4. Entropy per particle in the critical regime. (**A**) Entropy per particle S/N as a function of the scaled chemical potential $\tilde{\mu}$, measured in the temperature range of 5.8 to 15 nK (same symbol and color scheme as in Fig. 2A). (**B**) Critical entropy per particle S_c/N as a function of the effective interaction strength g: measurements for Bose gases with 2D optical lattices (black circle) and without lattice [black triangles, extracted from data in (*18*)], mean-field calculations (blue line), and a power-law fit to the measurements, $S_c/Nk_B = 1.6(1)g^{0.18(2)}$ (red line).

Equation of state measured near the quantum critical point can reveal essential information on quantum criticality, as proposed in (*28*).

We locate the quantum critical point by noting that at the critical chemical potential $\mu = \mu_0$, the scaled occupation number $\tilde{N} = Nt/k_BT = nd^2t/k_BT$ is temperature-independent, as indicated by Eq. 2. Here, we have applied a predicted exponent ν = 1/2. We plot $\tilde{N}$ as a function of μ in the low-temperature range of 5.8 to 15 nK, and indeed observe a crossing point at $\mu_0 = -4.5(6)t$ (Fig. 2A, inset). We identify this point as the critical point for the vacuum-to-superfluid transition, and our result agrees with the prediction $-4t$ (*28*).

To test the critical scaling law, we compare the equation of state at different temperatures. On the basis of the expected exponents z = 2 and ν = 1/2, we plot the scaled occupation number $\tilde{N}$ as a function of the scaled chemical potential $\tilde{\mu} = (\mu - \mu_0)/k_BT$ (Fig. 2A). Below 15 nK, all the measurements collapse into a single curve, confirming the emergence of the quantum critical scaling law (Eq. 2) at low temperatures. Note that we observe scaling behavior at temperatures from 5.8 to 15 nK, which are high compared to the tunneling scale t/k_B = 2.7 nK. Deviations become obvious at higher temperatures.

We examine the range of critical exponents z and ν that allow the scaled equation of state at low temperatures to overlap within experimental uncertainties. Taking $\mu_0 = -4.5t$ and various values of z and ν in the range of $0 < z < 4$ and $0 < \nu < 1$, we compute the corresponding scaled occupation numbers $\tilde{N}$ and scaled chemical potentials $\tilde{\mu}$ based on Eq. 3. We then evaluate how well the scaled equation of state in the range of T = 5.8 to 15 nK can collapse to a single curve by computing the reduced chi-squared (*30*). The best-fit exponents (Fig. 2B) are determined as $z = 2.2^{+1.0}_{-0.5}$ and $\nu = 0.52^{+0.09}_{-0.10}$, and the uncertainties correspond to a 95% confidence level. On the basis of the theoretical value of $\mu_0 = -4t$, we find the exponents to be $z = 2.6^{+1.2}_{-0.6}$ and ν = 0.44(8). In the following analyses, we adopt z = 2, ν = 1/2, and $\mu_0 = -4.5t$.

Our measurements at different temperatures allow us to investigate the breakdown of quantum criticality at high temperatures. To quantify the deviations, we focus on the temperature dependence of the scaled occupation number $\tilde{N}$ at the critical chemical potential $\mu = \mu_0$ (Fig. 3). Deviations from the low-temperature value are clear when the temperature exceeds $T^* = 22\,\text{nK} \approx 8t/k_B$. From this, we conclude that at $\mu = \mu_0$, the upper bound of thermal energy for the quantum critical behavior in our system is $k_BT^* \approx 8t$. Our result is in fair agreement with the prediction of $6t$ based on quantum Monte Carlo calculations (*23*).

From the equation of state, one can derive other thermodynamic quantities in the critical regime. We derive the entropy per particle S/N based on measurements in the temperature range of 5.8 to 15 nK, using a procedure similar to (*31*). The measured entropy per particle depends only on the scaled chemical potential $\tilde{\mu}$ and monotonically decreases (Fig. 4A), indicating a positive specific heat. Near the critical point $\tilde{\mu} = 0$, the entropy per particle has an approximate linear dependence on the scaled chemical potential: $S/Nk_B = a - b\tilde{\mu}$, with a = 1.8(1), b = 1.1(1). From this linear dependence, we derive an em-

pirical equation of state analogous to the ideal gas law (*30*)

$$P = Cn^{x}(k_{B}T)^{y} \quad (4)$$

where P is the pressure of the 2D gas, $x = 2/(1 + b) = 0.95(5)$, $y = 2b/(1 + b) = 1.05(5)$, $C = 0.8(2)(td^2)^w$ is a constant, and $w = (1 - b)/(1 + b) = -0.05(5)$.

Finally, we observe a weak dependence of the critical entropy per particle on the atomic interaction. Noting that a weakly interacting 2D Bose gas follows similar scaling laws near $\mu = 0$ (*18*) because it belongs to the same underlying dilute Bose gas universality class (*2*, *32*), we apply similar analysis and extract the critical entropy per particle S_c/N at four interaction strengths $g \approx 0.05$, 0.13, 0.19, 0.26, shown together with the lattice data ($g \approx 2.4$) in Fig. 4B. We observe a slow growing of S_c/N with g, and compare the measurements with mean-field calculations. The measured S_c/N is systematically lower than the mean-field predictions, potentially as a consequence of quantum critical physics. The weak dependence on the interaction strength can be captured by a power-law fit to the data as $S_c/Nk_B = 1.6(1)g^{0.18(2)}$.

In summary, on the basis of in situ density measurements of Bose gases in 2D optical lattices, we confirm the quantum criticality near the vacuum-to-superfluid quantum phase transition. Our experimental methods hold promise for identifying general quantum phase transitions, and prepare the tools for investigating quantum critical dynamics.

References and Notes

1. P. Coleman, A. J. Schofield, *Nature* **433**, 226 (2005).
2. S. Sachdev, *Quantum Phase Transitions* (Cambridge Univ. Press, Cambridge, 1999).
3. D. van der Marel *et al.*, *Nature* **425**, 271 (2003).
4. H. v. Löhneysen, A. Rosch, M. Vojta, P. Wölfle, *Rev. Mod. Phys.* **79**, 1015 (2007).
5. P. Gegenwart, Q. Si, F. Steglich, *Nat. Phys.* **4**, 186 (2008).
6. S. Sachdev, *Nat. Phys.* **4**, 173 (2008).
7. U. Al Khawaja, H. Stoof, *Nature* **411**, 918 (2001).
8. T. Senthil, A. Vishwanath, L. Balents, S. Sachdev, M. P. A. Fisher, *Science* **303**, 1490 (2004).
9. S. Sachdev, M. Müller, *J. Phys. Condens. Matter* **21**, 164216 (2009).
10. S. E. Sebastian *et al.*, *Nature* **441**, 617 (2006).
11. R. Coldea *et al.*, *Science* **327**, 177 (2010).
12. R. Jaramillo, Y. Feng, J. Wang, T. F. Rosenbaum, *Proc. Natl. Acad. Sci. U.S.A.* **107**, 13631 (2010).
13. M. Greiner, O. Mandel, T. Esslinger, T. W. Hänsch, I. Bloch, *Nature* **415**, 39 (2002).
14. K. Baumann, C. Guerlin, F. Brennecke, T. Esslinger, *Nature* **464**, 1301 (2010).
15. E. Haller *et al.*, *Nature* **466**, 597 (2010).
16. J. Simon *et al.*, *Nature* **472**, 307 (2011).
17. T. Donner *et al.*, *Science* **315**, 1556 (2007).
18. C.-L. Hung, X. Zhang, N. Gemelke, C. Chin, *Nature* **470**, 236 (2011).
19. R. Löw *et al.*, *Phys. Rev. A* **80**, 033422 (2009).
20. S. Trotzky *et al.*, *Nat. Phys.* **6**, 998 (2010).
21. Q. Zhou, T.-L. Ho, *Phys. Rev. Lett.* **105**, 245702 (2010).
22. K. R. A. Hazzard, E. J. Mueller, *Phys. Rev. A* **84**, 013604 (2011).
23. S. Fang, C.-M. Chung, P.-N. Ma, P. Chen, D.-W. Wang, *Phys. Rev. A* **83**, 031605(R) (2011).
24. Y. Kato, Q. Zhou, N. Kawashima, N. Trivedi, *Nat. Phys.* **4**, 617 (2008).
25. M. P. A. Fisher, P. B. Weichman, G. Grinstein, D. S. Fisher, *Phys. Rev. B* **40**, 546 (1989).
26. N. Gemelke, X. Zhang, C.-L. Hung, C. Chin, *Nature* **460**, 995 (2009).
27. C.-L. Hung, X. Zhang, N. Gemelke, C. Chin, *Phys. Rev. Lett.* **104**, 160403 (2010).
28. X. Zhang, C.-L. Hung, S.-K. Tung, N. Gemelke, C. Chin, *New J. Phys.* **13**, 045011 (2011).
29. B. Capogrosso-Sansone *et al.*, *New J. Phys.* **12**, 043010 (2010).
30. Materials and methods are available as supporting online material on *Science* Online.
31. T. Yefsah, R. Desbuquois, L. Chomaz, K. J. Günter, J. Dalibard, *Phys. Rev. Lett.* **107**, 130401 (2011).
32. S. Sachdev, E. R. Dunkel, *Phys. Rev. B* **73**, 085116 (2006).

Acknowledgments: We thank N. Prokof'ev and D.-W. Wang for discussions and numerical data; Q. Zhou, K. Hazzard, and N. Trivedi for discussions; and N. Gemelke and C. Parker for discussions and reading of the manuscript. The work was supported by NSF (grants PHY-0747907 and NSF-MRSEC DMR-0213745), the Packard foundation, and a grant from the Army Research Office with funding from the Defense Advanced Research Projects Agency Optical Lattice Emulator program. The data presented in this paper are available upon request sent to cchin@uchicago.edu.

Supporting Online Material

www.sciencemag.org/cgi/content/full/science.1217990/DC1
Materials and Methods
Fig. S1
References (*33*, *34*)

15 December 2011; accepted 30 January 2012
Published online 16 February 2012;
10.1126/science.1217990

Reactions of Solvated Electrons Initiated by Sodium Atom Ionization at the Vacuum-Liquid Interface

William A. Alexander,[1] Justin P. Wiens,[2] Timothy K. Minton,[1]* Gilbert M. Nathanson[2]*

Solvated electrons are powerful reagents in the liquid phase that break chemical bonds and thereby create additional reactive species, including hydrogen atoms. We explored the distinct chemistry that ensues when electrons are liberated near the liquid surface rather than within the bulk. Specifically, we detected the products resulting from exposure of liquid glycerol to a beam of sodium atoms. The Na atoms ionized in the surface region, generating electrons that reacted with deuterated glycerol, $C_3D_5(OD)_3$, to produce D atoms, D_2, D_2O, and glycerol fragments. Surprisingly, 43 ± 4% of the D atoms traversed the interfacial region and desorbed into vacuum before attacking C-D bonds to produce D_2.

Radiolysis experiments provide fundamental insights into electron reactivity in protic liquids such as water and alcohols through the use of ionizing reagents, including gamma rays and high-energy electrons, which penetrate deeply into solution. These reagents energize and ionize solvent molecules, creating hydrogen atoms and other free radicals, as well as solvated electrons, e_s^-, often in high enough concentrations to react with each other (*1*, *2*). Electrons and radicals created at the vacuum-liquid interface may behave differently from those in the bulk because of their partial solvation (*3*–*6*) and because transient neutral intermediates may evaporate before reacting further. Recent photoionization experiments show that partially to fully solvated electrons persist for $\geq 10^{-10}$ s at the surface of water, potentially leading to enhanced destruction of organic molecules in contact with these electrons (*6*–*8*). Molecular beam methods, using gas-phase sodium atoms as neutral precursors, provide a previously unexplored alternative for generating interfacial electrons in protic liquids. These electrons initiate a wide range of chemical events, including the production of atomic and molecular radicals that react at and near the surface or escape by evaporating from solution.

We performed the experiments by directing a weak effusive beam of sodium atoms at the surface of a liquid glycerol (1,2,3-propanetriol) film in vacuum. These Na atoms rapidly ionize into Na_s^+ and e_s^- in the interfacial region. We chose glycerol because of its low vapor pressure (10^{-4} torr) and water-like ability to solvate ions and electrons (*9*, *10*). Solvated electrons react in more diverse ways with alcohols than with water. In the latter case, the primary pathways are slow dissociation, $e_s^- + H_2O \rightarrow H + OH^-$, and fast recombination, $2e_s^- + 2H_2O \rightarrow H_2 + 2OH^-$ (*2*, *11*). The low flux of our effusive Na beam ensures that similar electron-electron recombination and additional radical-radical reactions do not compete with electron-solvent and radical-solvent reactions, whereas the soft landing and gentle ionization of Na generates elec-

[1]Department of Chemistry and Biochemistry, Montana State University, Bozeman, MT 59717, USA. [2]Department of Chemistry, University of Wisconsin, Madison, WI 53706, USA.

*To whom correspondence should be addressed. E-mail: tminton@montana.edu (T.K.M.); gmnathan@wisc.edu (G.M.N.)

Observation of Quantum Criticality with Ultracold Atoms in Optical Lattices

Xibo Zhang, Chen-Lung Hung, Shih-Kuang Tung, and Cheng Chin

Science, 335 (6072), • DOI: 10.1126/science.1217990

Critically Cold Atoms

Unlike classical phase transitions, such as the freezing of water into ice, which is driven by lowering the temperature of the system, quantum phase transitions occur at absolute zero and are driven by other parameters, including magnetic field or pressure. In the vicinity of a quantum phase transition, a critical region forms where physical observables obey scaling laws as a consequence of the self-similarity of the system. Quantum phase transitions and quantum criticality are usually observed in solid state, but Zhang *et al.* (p. 1070, published online 16 February) used an optical lattice filled with a cold gas of atoms to simulate a quantum phase transition—from an insulator to a superflnuid in two dimensions. They observed the characteristic scaling of the equation of state, a finding that will facilitate the building of a platform in a tunable system for further investigations of quantum criticality.